AIAA Aviation Forum and ASCEND co-located Conference Proceedings
29 July - 2 August 2024, Las Vegas, Nevada
AIAA AVIATION FORUM AND ASCEND 2024

10.2514/6.2024-4187

An orthogonal decomposition for nonlinear modal analysis

Tianyi Chu*
School of Computational Science & Engineering, Georgia Institute of Technology, 756 West Peachtree Street NW, Atlanta, GA 30332-4017, USA

Brandon C. Y. Yeung† and Oliver T. Schmidt‡
Department of Mechanical and Aerospace Engineering, Jacobs School of Engineering, UCSD, 9500 Gilman Drive, La Jolla, CA 92093-0411, USA

An orthogonal modal decomposition for identifying triadic interactions in fluid flows is presented. The decomposition is based on spectral momentum transfer and extracts coherent structures that partake in three-wave interactions and are optimal in terms of the third-order space-time flow statistics. The method distinguishes between two quadratically interacting components, one acting as a catalyst and the other as a donor of momentum, that collectively contribute to a tertiary component, the recipient. The resulting modes maximize the covariance between the donor and recipient for each triad. The method can be understood as an extension of bispectral mode decomposition (BMD) by considering the exact form of the quadratic nonlinearity of the Navier-Stokes equations. Unlike BMD, and more similar to classical proper orthogonal decomposition (POD), it provides ranked bases for the donor and recipient that are jointly optimal and orthonormal in their respective inner products. Two applications are considered: numerical data of a canonical unsteady cylinder wake and experimental data of a turbulent wind turbine wake by Biswas and Buxton [1].

I. Nomenclature

$\hat{\boldsymbol{c}}_{l\to n}, \boldsymbol{\psi}_{l\to n}$	=	convective/donor vector and basis
$(n-l, l, n)$	=	discrete indices for triadic interactions
$\boldsymbol{u}$	=	flow state
$\hat{\boldsymbol{r}}_n, \boldsymbol{\phi}_n$	=	recipient vector and basis
$\mathcal{R}\{\cdot\}$	=	real part
Re	=	Reynolds number
$\boldsymbol{S}$	=	two-point cross-bispectral correlation tensor
σ	=	singular value
St	=	Strouhal number
ω	=	angular frequency
$\boldsymbol{\Omega}$	=	computational domain
$\boldsymbol{x}$	=	spatial coordinates

Superscripts

$(\cdot)'$	=	fluctuating component
$\overline{(\cdot)}$	=	mean component
$\hat{(\cdot)}$	=	frequency-domain representation
$(\cdot)^{\mathrm{T}}$	=	transpose
$(\cdot)^{\mathrm{H}}$	=	Hermitian transpose
$(\cdot)^*$	=	complex conjugate

*Postdoctoral Fellow, School of Computational Science & Engineering, Member AIAA.
†Graduate Student, Department of Mechanical and Aerospace Engineering, Member AIAA.
‡Associate Professor, Department of Mechanical and Aerospace Engineering, Senior Member AIAA.

II. Introduction

The quadratic nonlinearity of the Navier–Stokes equations leads to triadic interactions, which constitute the fundamental mechanism for momentum and energy transfer in fluid flows. This is most obvious in Fourier space. Triadic interactions are prevalent in turbulent and transitional flows, giving rise to resonant mechanisms, energy cascades, and flow phenomena like harmonics. A well-established tool for analyzing triadic interactions in pointwise signals is bispectral analysis. It allows for the identification of the dominant triads as peaks in the bispectral density, which decomposes the signal's third-order moment, or skewness, into its frequency components. The reader is referred to the reviews [2–6] for further details on the bispectrum. The bispectrum, by definition, correlates two frequency components to their sum. Therefore, it can be used to identify triadic frequency interactions that satisfy the zero-sum condition. Generalizing the pointwise bispectrum to an integral measure of the bispectral density, Schmidt [7] introduced the bispectral mode decomposition (BMD) to identify the triadic interactions in the flow field through the phase-dependence of the involved frequency components. While BMD is based on temporal cross-correlation, the proposed method extracts spatiotemporal structures that optimally represent the contributions of triadically interacting frequency components based on spatial cross-correlation. For each given triad, we seek a pair of jointly optimal modal bases that optimally represent the covariance between donor and recipient frequency components identified from the form of the convective term. Computationally, this is achieved through a singular value decomposition (SVD) of the two-point cross-bispectral correlation tensor. The resulting convective term fields and recipient modes are orthonormal in their respective inner products and jointly provide the best representation of the third-order flow statistics. While the latter is a hallmark of BMD, the ability to generate a set of optimal basis vectors is a hallmark of classical proper orthogonal decomposition (POD, Lumley [8]), which provides a single modal basis that optimally represents the flow's second-order flow statistics. Unlike POD and BMD, however, it utilizes the form of the governing equations to attain its properties.

The remainder of this paper is organized as follows. Section III describes the governing equations and introduces the new orthogonal decomposition. Two applications of the decomposition are demonstrated in section IV: a cylinder wake (IV.A) and a wind turbine wake (IV.B). Section V discusses our findings and summarizes the method.

III. Methods

A. Spectral momentum transfer

The motion of an incompressible fluid is governed by the momentum equations,

$$\frac{\partial \boldsymbol{u}}{\partial t} = -(\boldsymbol{u}\cdot\boldsymbol{\nabla})\boldsymbol{u} - \boldsymbol{\nabla} p + \frac{1}{\mathrm{Re}}\nabla^2\boldsymbol{u}, \tag{1}$$

which have been nondimensionalized by the velocity scale, U_∞, the length scale, L, and are parameterized by the Reynolds number, Re. Assuming a time-periodic flow, the flow variables can be expanded as the Fourier series,

$$\boldsymbol{u}(\boldsymbol{x},t) = \sum_{n=-\infty}^{\infty} \hat{\boldsymbol{u}}_n(\boldsymbol{x})\mathrm{e}^{\mathrm{i}\omega_n t} \quad \text{and} \quad p(\boldsymbol{x},t) = \sum_{n=-\infty}^{\infty} \hat{p}_n(\boldsymbol{x})\mathrm{e}^{\mathrm{i}\omega_n t}. \tag{2}$$

For each angular frequency, ω_n, we obtain the frequency-domain representation of equation (1),

$$\mathrm{i}\omega_n\hat{\boldsymbol{u}}_n = -\Big(\widehat{(\boldsymbol{u}\cdot\boldsymbol{\nabla})\boldsymbol{u}}\Big)_n - \boldsymbol{\nabla}\hat{p}_n + \frac{1}{Re}\nabla^2\hat{\boldsymbol{u}}_n = -\sum_{l=-\infty}^{\infty} \underbrace{(\hat{\boldsymbol{u}}_{n-l}\cdot\boldsymbol{\nabla})\hat{\boldsymbol{u}}_l}_{\hat{\boldsymbol{c}}_{l\to n}} - \boldsymbol{\nabla}\hat{p}_n + \frac{1}{Re}\nabla^2\hat{\boldsymbol{u}}_n, \tag{3}$$

where in the second step we have invoked the convolution theorem. This frequency-domain, or spectral, momentum equation lies at the core of our modal momentum transfer analysis. For the often-used notation of triads, (k,l,n) with $k = n - l$, any two of the frequency components determine the remaining one. For simplicity, we use the pairwise notation (l,n) to denote the triplet $(n-l,l,n)$ in the following. For the case of $n = 0$, equation (3) simplifies to

$$0 = -(\bar{\boldsymbol{u}}\cdot\boldsymbol{\nabla})\bar{\boldsymbol{u}} - \sum_{l\neq 0} \underbrace{(\hat{\boldsymbol{u}}_{-l}\cdot\boldsymbol{\nabla})\hat{\boldsymbol{u}}_l}_{\hat{\boldsymbol{c}}_{l\to 0}} - \boldsymbol{\nabla}\bar{p} + \frac{1}{Re}\nabla^2\bar{\boldsymbol{u}} = -(\bar{\boldsymbol{u}}\cdot\boldsymbol{\nabla})\bar{\boldsymbol{u}} - \overline{(\boldsymbol{u}'\cdot\boldsymbol{\nabla})\boldsymbol{u}'} - \boldsymbol{\nabla}\bar{p} + \frac{1}{Re}\nabla^2\bar{\boldsymbol{u}}, \tag{4}$$

which are the Reynolds-averaged Navier-Stokes (RANS) equations, with $\boldsymbol{u}' \equiv \boldsymbol{u} - \bar{\boldsymbol{u}}$. The definition of $\boldsymbol{u}'$ implies that $\hat{\boldsymbol{u}}_l = \widehat{\boldsymbol{u}'_l}$ for $l \neq 0$, which leads to the second equality in equation (4). Each term in the RANS equations contributes

to the deformation of the mean flow, $\bar{\boldsymbol{u}}$. The term $\hat{\boldsymbol{c}}_{l\to 0}$, in particular, is responsible for momentum transfer via the Reynolds stress, $\overline{(\boldsymbol{u}'\cdot\boldsymbol{\nabla})\boldsymbol{u}'}$.

A wide variety of open flows exhibit strong convective instability. Examples encompass natural and technical flows, such as bluff-body wakes and boundary layers, as well as exogenously forced flows like plasma-induced jets. In these flows, the convective term $\hat{\boldsymbol{c}}_{l\to n}$ becomes dominant in both spectral momentum and kinetic energy equations. In the following, we outline how the spatial structures involved in spectral momentum transfer can be leveraged to identify and understand triadic flow interactions.

B. Modal decomposition

The goal of decomposition is to compute a pair of jointly optimal modal bases for a given triad, (l, n), such that the convective term, $\hat{\boldsymbol{c}}_{l\to n}$, and the recipient, $\hat{\boldsymbol{r}}_n$, are optimally represented in terms of covariance. We call the recipient $\hat{\boldsymbol{r}}$ instead of $\hat{\boldsymbol{u}}$ to account for the compressible case, where density is not constant. The kinetic energy of the convective term and the recipient are measured in the norm $\|\cdot\|$, induced by the inner product

$$\langle \boldsymbol{u}_1(\boldsymbol{x}), \boldsymbol{u}_2(\boldsymbol{x})\rangle = \int_\Omega \boldsymbol{u}_2^{\mathrm{H}}(\boldsymbol{x})\boldsymbol{u}_1(\boldsymbol{x})\,\mathrm{d}\boldsymbol{x}. \tag{5}$$

The optimal covariance is given by the optimization problem

$$\sigma = \max \frac{\mathrm{E}\left\{|\,\langle \hat{\boldsymbol{c}}_{l\to n}(\boldsymbol{x}), \hat{\boldsymbol{\psi}}_{l\to n}(\boldsymbol{x})\rangle\ \langle \hat{\boldsymbol{r}}_n(\boldsymbol{x}'), \hat{\boldsymbol{\phi}}_n(\boldsymbol{x}')\rangle^{\mathrm{H}}\,|\right\}}{\|\hat{\boldsymbol{\psi}}_{l\to n}(\boldsymbol{x})\|\,\|\hat{\boldsymbol{\phi}}_n(\boldsymbol{x}')\|} \tag{6a}$$

$$= \max \frac{\mathrm{E}\left\{\left|\left(\int_\Omega \hat{\boldsymbol{\psi}}_{l\to n}^{\mathrm{H}}(\boldsymbol{x})\hat{\boldsymbol{c}}_{l\to n}(\boldsymbol{x})\,\mathrm{d}\boldsymbol{x}\right)\left(\int_\Omega \hat{\boldsymbol{r}}_n^{\mathrm{H}}(\boldsymbol{x}')\hat{\boldsymbol{\phi}}_n(\boldsymbol{x}')\,\mathrm{d}\boldsymbol{x}'\right)\right|\right\}}{\|\hat{\boldsymbol{\psi}}_{l\to n}(\boldsymbol{x})\|\,\|\hat{\boldsymbol{\phi}}_n(\boldsymbol{x}')\|} \tag{6b}$$

$$= \max \frac{\mathrm{E}\left\{\left|\iint_\Omega \hat{\boldsymbol{\psi}}_{l\to n}^{\mathrm{H}}(\boldsymbol{x})\left(\hat{\boldsymbol{c}}_{l\to n}(\boldsymbol{x})\hat{\boldsymbol{r}}_n^{\mathrm{H}}(\boldsymbol{x}')\right)\hat{\boldsymbol{\phi}}_n(\boldsymbol{x}')\,\mathrm{d}\boldsymbol{x}\,\mathrm{d}\boldsymbol{x}'\right|\right\}}{\|\hat{\boldsymbol{\psi}}_{l\to n}(\boldsymbol{x})\|\,\|\hat{\boldsymbol{\phi}}_n(\boldsymbol{x}')\|} \tag{6c}$$

$$= \max \frac{\left|\iint_\Omega \hat{\boldsymbol{\psi}}_{l\to n}^{\mathrm{H}}(\boldsymbol{x})\boldsymbol{S}(\boldsymbol{x},\boldsymbol{x}')\hat{\boldsymbol{\phi}}_n(\boldsymbol{x}')\,\mathrm{d}\boldsymbol{x}\,\mathrm{d}\boldsymbol{x}'\right|}{\|\hat{\boldsymbol{\psi}}_{l\to n}(\boldsymbol{x})\|\,\|\hat{\boldsymbol{\phi}}_n(\boldsymbol{x}')\|}, \tag{6d}$$

where

$$\boldsymbol{S}(\boldsymbol{x},\boldsymbol{x}') = E\left\{\hat{\boldsymbol{c}}_{l\to n}(\boldsymbol{x})\hat{\boldsymbol{r}}_n^{\mathrm{H}}(\boldsymbol{x}')\right\} \tag{7}$$

represents the two-point cross-bispectral correlation tensor for each $(n-l, l)$. This tensor is a Fredholm kernel, and the modes that jointly maximize σ can be obtained via the singular value expansion (SVE) of $\boldsymbol{S}$ [9], that is

$$\boldsymbol{S}(\boldsymbol{x},\boldsymbol{x}') = \sum_{j=1}^{\infty} \sigma_j \hat{\boldsymbol{\psi}}_{l\to n,j}(\boldsymbol{x})\hat{\boldsymbol{\phi}}_{n,j}^{\mathrm{H}}(\boldsymbol{x}') \quad \text{for each} \quad (n-l, l). \tag{8}$$

The convective term field, $\hat{\boldsymbol{\psi}}_{l\to n,j}$, and recipient mode, $\hat{\boldsymbol{\phi}}_{n,j}$, are ordered by their associated singular values, $\sigma_1 \geq \sigma_2 \geq \cdots \geq 0$. They are also orthogonal in their respective inner products and have unit energy,, that is, $\left\langle \hat{\boldsymbol{\psi}}_{l\to n,i}, \hat{\boldsymbol{\psi}}_{l\to n,j}\right\rangle = \left\langle \hat{\boldsymbol{\phi}}_{n,j}, \hat{\boldsymbol{\phi}}_{n,j}\right\rangle = \delta_{ij}$. In practice, that is for discrete data, equation (8) is solved by the singular value decomposition. In the special case where the convective term is identical to the recipient, $\hat{\boldsymbol{c}}_{l\to n} = \hat{\boldsymbol{r}}_n$, equations (6-8) reduce to the proper orthogonal decomposition framework by Lumley [8, 10]. By defining the expansion coefficients,

$$a_j = \left\langle \hat{\boldsymbol{r}}_n, \hat{\boldsymbol{\phi}}_{n,j}\right\rangle, \quad \text{and} \quad b_j = \left\langle \hat{\boldsymbol{c}}_{l\to n}, \hat{\boldsymbol{\psi}}_{l\to n,j}\right\rangle, \tag{9}$$

equation (6) can be recast as

$$\sigma_j = \max \mathrm{E}\{|b_j a_j^*|\}, \tag{10}$$

which maximizes the covariance between the projections of the convective term and the recipient onto their respective modal bases. In this form, the method can be seen as a specialized version of maximum covariance analysis (MCA) [11].

MCA and the closely related canonical correlation analysis (CCA) [12] identify bases that are jointly optimal in terms of multivariate statistics and have been widely used in data mining. For more details of CCA and its variants, readers are referred to [13–15]. We note that a and b need not be explicitly computed in the momentum transfer analysis. For each triad, the optimal expansion coefficients satisfy

$$\mathrm{E}\{|b_j a_k^*|\} = \sigma_j \delta_{jk}, \tag{11}$$

that is, the coefficients are uncorrelated with one another.

IV. Applications

Flow	Method	Re	Flow type	Fundamental frequency	Sec.
Cylinder wake	DNS [16]	100	2D laminar	$St_0 = 0.165$	§IV.A
Wind turbine wake	TR-PIV [1, 17]	$\approx 4 \times 10^4$	2D turbulent	$St_0 = 1.87$	§IV.B

Table 1 Overview of datasets.

We demonstrate the decomposition framework using two representative examples: canonical unsteady cylinder wake and turbulent PIV data of a wind turbine wake, as summarized in table 1. These two examples are benchmark problems for convective flows and are appropriate for demonstrating triadic interactions. The rotational frequency is considered the fundamental frequency of the wind turbine wake.

A. Cylinder wake

We first consider a canonical unsteady cylinder wake at a Reynolds number, based on the cylinder diameter and the free-stream velocity, of Re = 100. Jin et al. [18] have conducted triadic interactions and energy transfer analysis for this specific cylinder wake through resolvent analysis. They computed the convective terms and transfers using optimal resolvent modes, but this approach resulted in a loss of optimality in terms of triadic interactions. On the other hand, the proposed decomposition framework specifically addresses this need. The direct numerical simulation (DNS) data of the unsteady cylinder flow is obtained using the PHS+poly RBF-FD version of the fractional-step, staggered-grid incompressible Navier-Stokes solver [16]. The cylinder is located at the origin with a diameter of 1. The time step is adjusted in the simulation to ensure that the Fourier block with a size of $N = 1200$ is able to capture multiple complete flow cycles. The flow fields are interpolated on a Cartesian mesh within the computational domain $\Omega = [x, y] \in [-5,\ 30] \times [-5,\ 5]$.

Figure 1 shows the leading mode bispectrum. Local maxima appear at integer multiples of the fundamental vortex shedding frequency, which is $St_0 = 0.165$ [19–21]. These maxima indicate the most dominant triadic interactions within the cylinder wake and represent a cascade of triads.

Several active triads can be observed along the lines, $St_l = St_n$ and $St_n = 0$. The former represents the advection of harmonics. The latter suggests that the spatial deformation of the mean flow field is mainly generated by the fundamental difference-self-interaction, that is, the interactions between the harmonics and their corresponding conjugates. In this case, the intrinsic instability mechanism associated with the mean flow distortion is the vortex shedding behind the bluff-body. Besides, the sum-interaction of the fundamental instability with itself that generates the second harmonic, i.e., $(St_l, St_n) = (St_0, 2St_0)$, is also well-captured by the current framework.

Figure 2 shows the leading modes for different interactions. Due to the intrinsic bluff-body vortex shedding instability mechanisms, the leading recipient modes are identical for different donor frequencies. The convective term fields, however, are different for the same recipient frequency. This indicates that different triadic interactions contribute to the same instability mechanism. Meanwhile, all the convective term fields only have downstream spatial support, as compared to the adjoint modes obtained using classical linear stability analysis [22] and the forcing modes using resolvent analysis [18, 23, 24], respectively, which are active far upstream of the cylinder. This observation implies that the current framework addresses a critical gap left by these linear analyses. These analyses, by construction, are insufficient to capture the complete convective instability mechanism owing to its intrinsic quadratic nonlinearity.

The transfer fields describe the entire spatial interactions between the convective term fields and the recipient modes. It is worth noting that these transfer fields have compact support, even though the donor and recipient modes are active far downstream of the cylinder. This suggests that the most important triadic interactions are taking place closely

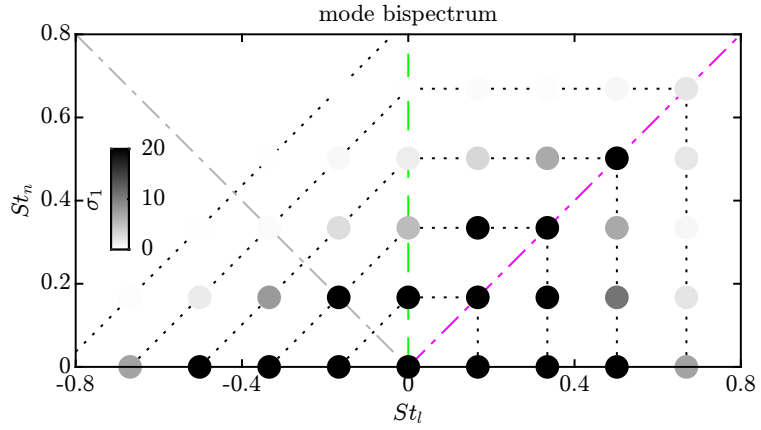

Fig. 1 Leading mode bispectrum of the cylinder wake at Re=100. Different donor-recipient combinations are marked as $l = n$ (magenta), $l = 0$ (green), and $l + n = 0$ (gray).

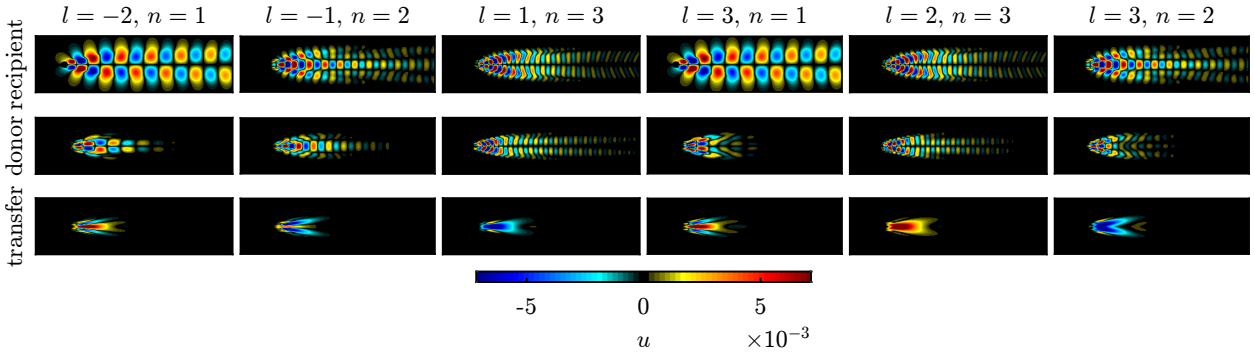

Fig. 2 Streamwise velocity component of the leading modes of the cylinder wake: (row 1) recipient mode; (row 2) donor field; (row 3) transfer field. Each column corresponds to a triad in the mode bispectrum of figure 1, and the indices l and n represent the integer multiples of the vortex shedding frequency. The shown computational domain is $\Omega = [-5,\ 30] \times [-5,\ 5]$.

downstream of the cylinder. This observation is consistent with the experimental-based structural perturbation analysis [25] and the predicted-based wavemaker analysis [22, 26]. The latter is a linear approach that identifies the flow region with the strongest localized feedback, where the dominant instability mechanisms are at work. Beyond linear analysis, the transfer fields now capture these regions by optimally accounting for the actual triadic interactions.

B. Wind turbine wake

In the second application, we demonstrate the utility of the new orthogonal decomposition for the identification of dominant triads in experimental data of turbulent flows. We choose the example of the turbulent wake of a model wind turbine from Biswas and Buxton [1, 17], with a Reynolds number of 40000 based on the rotor diameter and freestream velocity. The turbine wake flow exemplifies real-world data of mixed broadband-tonal turbulent flows, whose complex dynamics exhibits both stochastic and deterministic behaviors, in the presence of noise and other measurement artifacts. The data were captured using time-resolved particle image velocimetry (TR-PIV), and correspond to experiment 1A in Biswas and Buxton [17]. The field of view (FOV) of the PIV is aligned with the axis of the turbine tower, and spans $x/D \in [0.5, 5]$ and $y/D \in [-0.35, 0.75]$ in the streamwise and transverse directions, respectively, where D is the diameter of the rotor. The rotor revolves at a tip speed ratio of $\lambda = \pi St_0 \approx 6$, where $St_0 = f_0 D/U_\infty = 1.87$ is the rotational frequency and U_∞ is the freestream velocity. The time series consists of 5456 snapshots separated by a constant spacing of $\Delta t U_\infty/D = 0.01$, and spans 102 revolutions. The period of each revolution is given by $TU_\infty/D = 1/St_0 = 0.535$. The three-bladed rotor also imposes a blade-passing frequency (BPF) of $3St_0 = 5.61$ on the flow. Biswas and Buxton [17] previously analyzed this flow using the technique of optimal mode decomposition

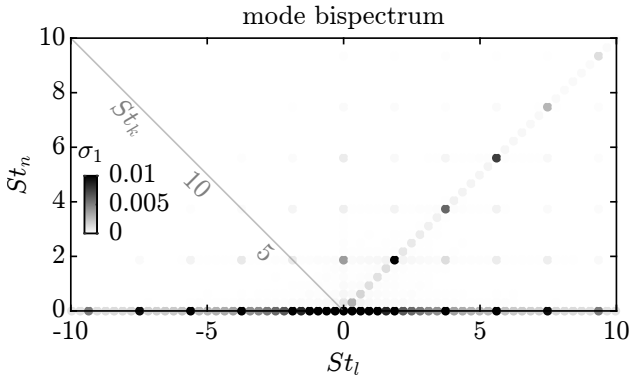

Fig. 3 Leading mode bispectrum of the turbine wake.

(OMD; [27]), itself an extension to dynamic mode decomposition (DMD; [28]). They extracted coherent structures using OMD, then projected the kinetic energy budget equation onto the dominant structures, finding significant energy transfer among St_0, $3St_0$, and their harmonic peaks via triadic interactions. The turbine wake is thus ideal for assessing the new orthogonal decomposition, which, distinct from OMD or DMD, directly and optimally accounts for triads.

For spectral estimation, we choose a block size of $N_f = 321$, equivalent to six rotational periods, and use a rectangular window. As with the cylinder wake in section IV.A, this combination of parameters ensures that the discrete spectral energy distribution of the turbine wake is accurately captured. Figure 3 shows the leading mode bispectrum computed using the orthogonal decomposition. As expected, the mode bispectrum reveals a grid-like pattern of local maxima, which identify triads made up of St_0 and its harmonic frequencies. The most dominant triads are found along the $St_n = 0$ axis. Each of these triads corresponds to the convective term $\hat{\boldsymbol{c}}_{l\to 0}$ within the RANS equations in (4). They thus conspire to deform the turbulent mean flow through the action of the Reynolds stress, $\overline{(\boldsymbol{u}' \cdot \boldsymbol{\nabla})\boldsymbol{u}'}$. An example is the triad $(St_l, St_n) = (St_0, 0)$, whose corresponding leading modes are reported in figure 4(a,b). The recipient mode, $\hat{\boldsymbol{\phi}}_n$, as expected, recovers the mean flow. Its magnitude peaks in the region $y < 0$, near the tower of the wind turbine. The donor field, $\hat{\boldsymbol{\psi}}_{l\to n}$, on the other hand, resembles elongated, streak-like structures along the tip of the rotor, $y = 0.5$. These structures represent momentum transfer to and from the mean flow through the unsteady tip vortex shedding.

The diagonal line representing $St_n = St_l$, or equivalently, $St_k = 0$, also displays active triad interactions. Along this line, the local maxima correspond to the term $\hat{\boldsymbol{c}}_{n\to n}$ in the spectral momentum equation (3), with St_n equal to the harmonic frequencies. From the form of the convective term, it can be inferred that these triads arise due to advection of the harmonics by the mean flow. The dominance of these triads in the mode bispectrum reflects the convective nature of wake flows, including both cylinder and turbine wakes. The most active of these triads are $(St_l, St_n) = (St_0, St_0)$ and $(3St_0, 3St_0)$. They couple the mean flow to the exogenous forcing, i.e., the rotational and blade-passing frequencies, St_0 and $3St_0$, respectively. The donor field and recipient mode of the triad $(St_l, St_n) = (St_0, St_0)$ are visualized in figure 4(d,e). They both show the convection of the tip vortices along the tip shear layer at the rotational frequency, and are in excellent agreement with the OMD modes of Biswas and Buxton [17].

Triad interactions that do not involve the mean flow as one frequency component are also clearly identified in the mode bispectrum, but are considerably weaker than those that do. This signifies that the overall dynamics of the flow are biased towards linear rather than nonlinear mechanisms. The modes for two such triads, $(St_l, St_n) = (2St_0, 3St_0)$ and $(St_l, St_n) = (3St_0, 2St_0)$, are shown in figure 4(j,k) and (m,n), respectively. By contrast, the nonlinear and linear triads appear balanced for the cylinder wake in figure 1. Unlike the laminar cylinder wake, the mode bispectrum of the turbulent turbine wake also shows nonzero singular values at non-harmonic frequencies, providing evidence of triadic interactions even within the stochastic turbulence. Non-harmonic modes are exemplified by the triad $(St_l, St_n) = (0.93, 0.93)$ shown in figure 4(p,q). Distinct from the tip vortex modes, this low-frequency mode has instead been linked to shedding from the turbine tower [17]. The lack of well-defined wavepacket structures is consistent with the broadband nature of this region of the mode bispectrum in figure 3. Another notable difference from the tip vortex modes is the spatial support of the low-frequency mode, which persists to large x and appears to experience spatial growth far downstream of the turbine.

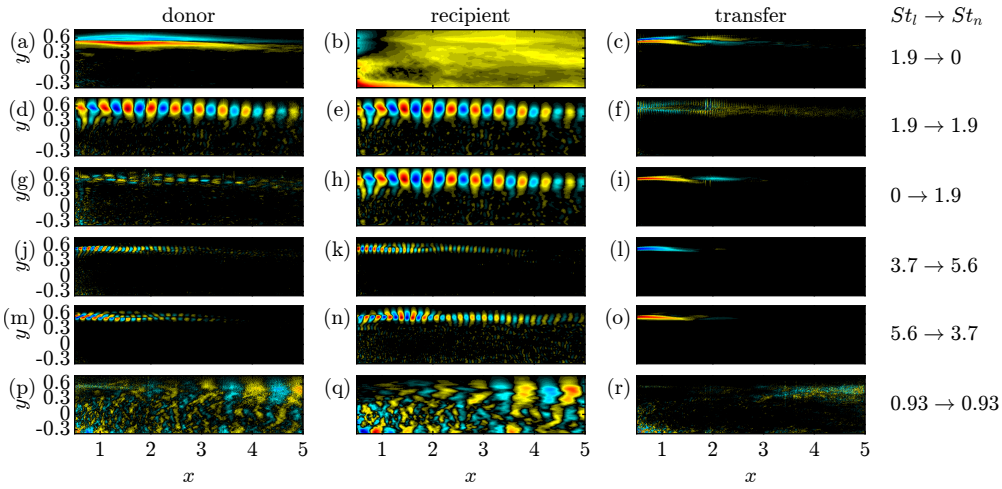

Fig. 4 Transverse velocity component of the leading modes of the turbine wake: (a,d,g,j,m,p) donor field; (b,e,h,k,n,q) recipient mode; (c,f,i,l,o,r) transfer field. Each row corresponds to a triad in the mode bispectrum of figure 3.

V. Summary

We have demonstrated the new orthogonal decomposition on two examples. The first is DNS data of a laminar unsteady cylinder wake, which is a benchmark problem for canonical convective flows characterized by well-understood nonlinear dynamics. The mode bispectrum analysis indicates that the most dominant triadic interactions occur at integer multiples of the fundamental vortex shedding frequency. Additionally, it reveals that the intrinsic bluff-body vortex-shedding instability mechanism is primarily caused by the interactions between the harmonics and their corresponding conjugates. Unlike the flow structures predicted by linear analyses, which neglect the quadratic nonlinearity within the convective terms, the donor fields exhibit purely downstream spatial support. This means that the upstream structures in adjoint or forcing modes are purely mathematical results obtained from the eigen- or singular-decomposition of the linearized Navier-Stokes operator. They are not active in the actual triadic interactions. The transfer fields between the donor and recipient modes indicate that the most significant triadic interactions occur in close proximity to the cylinder. This aligns with the structural perturbation analysis based on experiments.

The second example is TR-PIV data of a turbulent wind turbine wake. This flow is characterized by both deterministic and stochastic components. Moreover, the case is representative of experimental data that are inevitably contaminated by measurement noise. The mode bispectrum successfully identifies dominant triads made up of the harmonics of the rotor rotational frequency. The modes reveal vortex shedding from the rotor tips as well as from the turbine tower. As is almost always the case with experimental diagnostics, some information is lost when two-dimensional data are captured from a statistically three-dimensional flow, such as the turbine wake. This inherently limits the terms in the momentum equations that can be modeled using the new decomposition. In particular, out-of-plane velocity and velocity gradients, which contribute to momentum transfer, cannot be included in the analysis. That the method nevertheless succeeds in uncovering the nonlinear dynamics of the turbine wake supports its broad applicability to data sets in which the full flow state is only partially observable.

References

[1] Biswas, N., and Buxton, O. R. H., "Effect of tip speed ratio on coherent dynamics in the near wake of a model wind turbine," *J. Fluid Mech.*, Vol. 979, No. A34, 2024, pp. 1–31.

[2] Collis, W. B., White, P. R., and Hammond, J. K., "Higher-order spectra: the bispectrum and trispectrum," *Mech. Syst. Signal Process*, Vol. 12, No. 3, 1998, pp. 375–394.

[3] Kim, Y. C., and Powers, E. J., "Digital bispectral analysis and its applications to nonlinear wave interactions," *IEEE Trans. Plasma Sci.*, Vol. 7, No. 2, 1979, pp. 120–131.

[4] Brillinger, . R., "An introduction to polyspectra," *Ann. Math. Stat.*, Vol. 36, 1965, pp. 1351–1374.

[5] Nikias, C. L., and Raghuveer, M. R., "Bispectrum estimation: A digital signal processing framework," *Proc. IEEE*, Vol. 75, No. 7, 1987, pp. 869–891.

[6] Nikias, C. L., and Mendel, J. M., "Signal processing with higher-order spectra," *IEEE Signal Process. Mag.*, Vol. 10, No. 3, 1993, pp. 10–37.

[7] Schmidt, O. T., "Bispectral mode decomposition of nonlinear flows," *Nonlinear Dyn.*, Vol. 102, No. 4, 2020, pp. 2479–2501.

[8] Lumley, J. L., "The structure of inhomogeneous turbulent flows," *Atmospheric turbulence and radio wave propagation*, 1967.

[9] Schmidt, E., "Zur Theorie der linearen und nichtlinearen Integralgleichungen," *Math. Ann.*, Vol. 63, No. 4, 1907, pp. 433–476.

[10] Lumley, J. L., *Stochastic tools in turbulence*, Academic Press, New York, 1970.

[11] Von Storch, H., and Zwiers, F. W., *Statistical analysis in climate research*, Cambridge university press, 1999.

[12] Hotelling, H., "Relations between two sets of variates," *Breakthroughs in statistics: methodology and distribution*, Springer, 1992, pp. 162–190.

[13] Thompson, B., *Canonical correlation analysis: Uses and interpretation*, 47, Sage, 1984.

[14] Hardoon, D. R., Szedmak, S., and Shawe-Taylor, J., "Canonical correlation analysis: An overview with application to learning methods," *Neural Comput.*, Vol. 16, No. 12, 2004, pp. 2639–2664.

[15] Andrew, G., Arora, R., Bilmes, J., and Livescu, K., "Deep canonical correlation analysis," *ICML*, PMLR, 2013, pp. 1247–1255.

[16] Chu, T., and Schmidt, O. T., "RBF-FD discretization of the Navier-Stokes equations on scattered but staggered nodes," *J. Comput. Phys.*, Vol. 474, 2023, p. 111756.

[17] Biswas, N., and Buxton, O. R. H., "Energy exchanges between coherent modes in the near wake of a rotor model at different tip speed ratios," *arXiv preprint arXiv:2402.13063*, 2024.

[18] Jin, B., Symon, S., and Illingworth, S. J., "Energy transfer mechanisms and resolvent analysis in the cylinder wake," *Phys. Rev. Fluids*, Vol. 6, No. 2, 2021, p. 024702.

[19] Williamson, C. H. K., "Defining a universal and continuous Strouhal–Reynolds number relationship for the laminar vortex shedding of a circular cylinder," *Phys. Fluids*, Vol. 31, No. 10, 1988, pp. 2742–2744.

[20] Barkley, D., "Linear analysis of the cylinder wake mean flow," *Europhys. Lett.*, Vol. 75, No. 5, 2006, p. 750.

[21] Jiang, H., and Cheng, L., "Strouhal–Reynolds number relationship for flow past a circular cylinder," *J. Fluid Mech.*, Vol. 832, 2017, pp. 170–188.

[22] Marquet, O., Sipp, D., and Jacquin, L., "Sensitivity analysis and passive control of cylinder flow," *J. Fluid Mech.*, Vol. 615, 2008, pp. 221–252.

[23] Symon, K., S.and Rosenberg, Dawson, S. T. M., and McKeon, B. J., "Non-normality and classification of amplification mechanisms in stability and resolvent analysis," *Phys. Rev. Fluids*, Vol. 3, No. 5, 2018, p. 053902.

[24] Chu, T., and Schmidt, O. T., "Mesh-free hydrodynamic stability," *J. Comput. Phys.*, Vol. 502, 2024, p. 112822.

[25] Strykowski, P. J., and Sreenivasan, K. R., "On the formation and suppression of vortex 'shedding'at low Reynolds numbers," *J. Fluid Mech.*, Vol. 218, 1990, pp. 71–107.

[26] Giannetti, F., and Luchini, P., "Structural sensitivity of the first instability of the cylinder wake," *J. Fluid Mech.*, Vol. 581, 2007, pp. 167–197.

[27] Wynn, A., Pearson, D. S., Ganapathisubramani, B., and Goulart, P. J., "Optimal mode decomposition for unsteady flows," *J. Fluid Mech.*, Vol. 733, 2013, pp. 473–503.

[28] Schmid, P. J., "Dynamic mode decomposition of numerical and experimental data," *J. Fluid Mech.*, Vol. 656, 2010, pp. 5–28.